# Coherent Manipulation of Electron Spins up to Ambient Temperatures in $Cr^{5+}(S = 1/2)$ Doped $K_3NbO_8$

S. Nellutla,[1] K.-Y. Choi,[1,2] M. Pati,[2] J. van Tol,[1,2] I. Chiorescu,[1,3] and N. S. Dalal[1,2]

[1]*National High Magnetic Field Laboratory, Tallahassee, Florida 32310, USA*
[2]*Department of Chemistry and Biochemistry, Florida State University, Tallahassee, Florida 32306-4390, USA*
[3]*Department of Physics, Florida State University, Tallahassee, Florida 32306-4350, USA*

(Received 19 March 2007; published 24 September 2007)

We report coherent spin manipulation on $Cr^{5+}$ ($S = 1/2$, $I = 0$) doped $K_3NbO_8$, which constitutes a dilute two-level model relevant for use as a spin qubit. Rabi oscillations are observed for the first time in a spin system based on transition metal oxides up to room temperature. At liquid helium temperature the phase coherence relaxation time $T_2$ reaches $\sim 10$ $\mu$s and, with a Rabi frequency of 20 MHz, yields a single-qubit figure of merit $Q_M$ of about 500. This shows that a diluted ensemble of $Cr^{5+}$ ($S = 1/2$) doped $K_3NbO_8$ is a potential candidate for solid-state quantum information processing.

DOI: 10.1103/PhysRevLett.99.137601 PACS numbers: 76.30.Fc, 03.67.Lx, 72.80.Ga

Recently, electron spins in solids have been intensively discussed in terms of physical implementations of a quantum computer [1] and several proposals for embodying solid-state spin qubits have been put forward. The discussed physical systems comprise quantum dots [2–4], phosphorous donors in silicon [5], endohedral fullerenes [6], nitrogen-vacancy centers in diamond [7–11], molecular magnets [12,13], and rare-earth ions [14]. They commonly make use of the well-characterized discrete energy levels arising from the spin, orbital, or charge states. Even though transition metal ions have these states, to our knowledge, they have not been exploited as a basic building block of solid-state spin qubits. More importantly, they could be made essentially free of magnetic anisotropy and therefore suitable for on-chip deposition and spin manipulation (*vide infra*).

In this Letter, we explore this possibility by lightly doping a $S = 1/2$ $Cr^{5+}$ ion into the nonmagnetic matrix of $K_3NbO_8$. Cr was chosen since its dominant isotope $^{52}Cr$ (90.5% natural abundance) has nuclear spin $I = 0$, thus obviating complications like spin decoherence due to hyperfine interactions. A further advantage of this system is that, in principle, it can be isotopically enriched with $^{53}Cr$ ($I = 3/2$, 9.5% natural abundance) to produce a potential multiqubit system. We observed Rabi oscillations of the $S = 1/2$ and $I = 0$ Cr spin in a wide temperature range of 4 to 290 K and almost independent of field orientation. The measured spin dephasing times and ease of material synthesis suggest that such spin qubits based on transition metal oxides might be suitable for scalable quantum computing.

Cr doped $K_3NbO_8$ (hereafter Cr:$K_3NbO_8$) crystallizes in a tetragonal unit cell ($I\bar{4}2m$) with lattice parameters $a = 6.694$ Å and $c = 7.574$ Å. Figure 1(a) shows a schematic of the Cr:$K_3NbO_8$ system. $Nb^{5+}$ ions are shown at the corners while the $Cr^{5+}$ ion is shown at the body center position. Single crystals of Cr:$K_3NbO_8$ were prepared as described elsewhere [15,16] and the $Cr^{5+}$ concentration was determined to be $\sim 0.03\%$ in the studied sample. Electron paramagnetic resonance (EPR) measurements were performed using a Bruker Elexsys 680 spectrometer at $X$ band ($\nu \sim 9.64$ GHz) in both continuous-wave (cw) and pulsed modes. Temperature was varied between 4 and 290 K using helium-flow cryostat.

The electronic spin Hamiltonian for Cr:$K_3NbO_8$ can be written as follows:

$$\hat{H} = \mu_B B_0 \cdot \mathbf{g} \cdot \hat{S} + \hat{H}_{\rm hf} + \hat{H}_{\rm dipole}. \quad (1)$$

The first term is the electron Zeeman interaction where $\mu_B$ is the Bohr magneton, $\mathbf{g}$ the $g$ tensor, and the $\hat{S}$ the spin operator. $\hat{H}_{\rm hf}$ comprises the hyperfine interactions given by

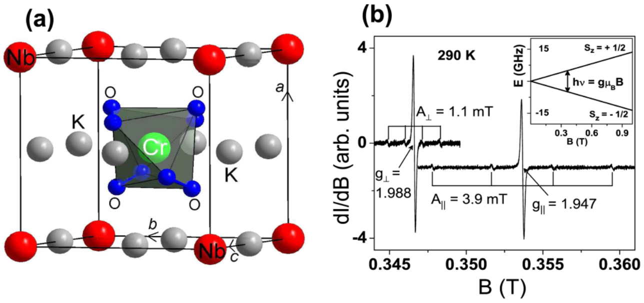

FIG. 1 (color online). (a) Crystal structure of $Cr^{5+}$ doped $K_3NbO_8$: Cr [green (or light gray) ball], Nb [red (or dark gray) balls], K (gray balls), and O [blue (or black) balls]. For clarity, the oxygen atoms are shown only around the Cr ion (dark gray polyhedron). (b) Room temperature cw EPR spectra (vertically shifted for clarity) measured at $\nu \sim 9.64$ GHz for $B_0 \perp c$ and $B_0 \| c$, respectively. In both cases, the strong central peak corresponds to the $S = 1/2$, $I = 0$ resonance and the four weak sidebands are due to the $^{53}Cr$ isotope ($I = 3/2$, 9.5% natural abundance). The inset displays the energy level diagram showing the eigenstates of the $S = 1/2$, $I = 0$ spin system in an external field.

$\sum_n \hat{S} \cdot \mathbf{A} \cdot \hat{I}^n$. Even though there are no hyperfine interactions with the $^{52}$Cr ($I = 0$) nuclei, we have found that the superhyperfine interactions from $^{39}$K nuclei ($I = 3/2$, 93.3% natural abundance) are non-negligible and also the interactions with the $^{93}$Nb ($I = 9/2$, 100% natural abundance) cannot be ruled out. The third term represents the dipolar interactions between electron spins. In solids, dipolar coupling is usually the principal mechanism limiting the spin-spin relaxation time $T_2$. However, in our case ($\sim$0.03% $Cr^{5+}$ concentration), a mean separation of $\sim$8 nm between $Cr^{5+}$ ions yields an average electron-electron dipolar interaction of about 0.1 MHz. Our system is sufficiently diluted that it can be considered as an almost perfectly isolated Kramer's spin $S = 1/2$ system.

cw EPR spectra of the Cr:$K_3NbO_8$ single crystal recorded at room temperature are presented in Fig. 1(b). The single central peak corresponds to the electron-spin transition $\Delta S_z = \pm 1$ within the $S = 1/2, I = 0$ doublet, as shown in the inset. The $g$ values correspond to $g_\perp = 1.9878 \pm 0.0002$ for $B_0 \perp c$ and $g_\parallel = 1.9472 \pm 0.0002$ for $B_0 || c$ and are characteristic of a tetragonally distorted tetrahedral system with a $3d_{x^2-y^2}$ ground state [16]. We note that the $g$ anisotropy in our system is small and therefore can be treated as quasi-isotropic. The four weak satellite peaks flanking the central line for both orientations arise from the hyperfine coupling to the nuclear spin $I = 3/2$ of the $^{53}$Cr isotope with $A_\parallel = 3.9 \pm 0.1$ mT and $A_\perp = 1.1 \pm 0.1$ mT. In this study, we will address only the central resonance from the $S = 1/2$, $I = 0$ $^{52}$Cr single-qubit spin system.

As a first step, the two important characteristics of a qubit, namely, the spin-lattice relaxation time ($T_1$) and the spin-spin relaxation ($T_2$) time, were measured using the standard pulse sequences. $T_1$ was measured by an inversion-recovery [using free induction decay (FID)] method employing the sequence $\pi$-$\tau$-$\pi/2$-FID with varying $\tau$. $T_1$ increases continually from $\sim$526 ns at room temperature to $\sim$1 s at 4 K. This indicates that the spin-lattice relaxation is caused by thermal processes. $T_2$ is obtained using a 2-pulse Hahn echo decay sequence $\pi/2$-$\tau$-$\pi$-echo that gives the echo intensity as a function of $\tau$ [see Fig. 2(a)]. The observed oscillations are from the electron-spin echo envelope modulation (ESEEM) effect. Their Fourier transform yields the $^{39}$K nuclear spin levels splittings due to the combined effect of nuclear Zeeman, superhyperfine, and quadrupole interactions. An electron nuclear double resonance study at 240 GHz [17] yields the hyperfine couplings which range from 0.41–0.73 MHz and which are consistent with the ESEEM results. These values allow us to assign the Gaussian line shape and the linewidth (4.2 MHz) of the EPR resonance to the unresolved superhyperfine coupling with the surrounding K nuclei. For a Gaussian line, the relation between the FID decay time $T_2^*$ and the linewidth $\Delta B_{pp}$ is given as $T_2^* = 2\sqrt{2}/\Delta B_{pp}$. Using the above mentioned $\Delta B_{pp}$ of 4.2 MHz, $T_2^*$ can be estimated as $\sim$108 ns.

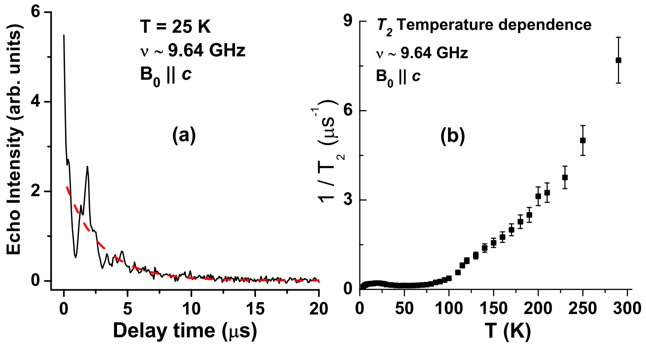

FIG. 2 (color online). (a) Hahn echo intensity decay of Cr:$K_3NbO_8$ as a function of delay time at $\nu \sim 9.64$ GHz and 25 K for $B_0 || c$. Observed modulation of the echo height is due to the superhyperfine coupling with the $^{39}$K nuclei. The dashed line is the exponential fit to extract spin-spin relaxation time $T_2$. (b) Temperature dependence of $T_2$ for $B_0 || c$ at $\nu \sim 9.64$ GHz.

The temperature dependence of $T_2$ for $B_0 || c$ at $\sim$9.64 GHz is displayed in Fig. 2(b). $T_2$ slowly increases from $\sim$130 ns at room temperature to $\sim$10 $\mu$s at 70 K and essentially remains constant down to 4 K. The details will be discussed in a separate paper [17].

The decay of the macroscopic magnetic moment perpendicular to the magnetic field due to the dephasing of the individual spin packets with respect to each other is measured by the FID and is shown in Fig. 3(a). Here, we plot the FID measured at 4.2 K for two detuning fields $\delta B$ ($= B_0 - B_{\rm res}$) for $B_0 || c$-axis orientation. In a rotating frame of reference [18], $B_0$ is along the $z$ axis, whereas $B_1$ is along the $x$ axis. A $\pi/2$ pulse applied with a $+x$ phase

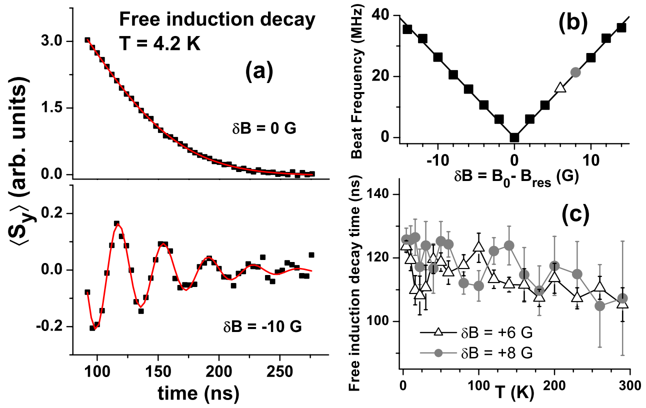

FIG. 3 (color online). (a) $Cr^{5+}$ free induction decay (FID) at 4.2 K for two values of applied magnetic field $B_0 = B_{\rm res} + \delta B$, with $B_{\rm res}$ determined from the cw resonance experiment for $B_0 || c$ [see Fig. 1(b)]. Experimental data (squares) are well fitted by a damped oscillatory motion (solid lines). (b) The beat frequency of the FID versus detuning field. The data are well described by a through-origin linear fit. (c) The total dephasing time ($T_2{}^*$) as a function of temperature for two values of $\delta B$ [shown in (b) by a triangle and a full circle]. $T_2^*$ remains practically constant from 4.2 K to room temperature.

rotates the spins, initially aligned along the $z$ axis, to the $-y$ axis and when on-resonance ($B_0 = B_{\mathrm{res}}$), the spins remain oriented along the $-y$ axis during the free evolution period and decay with $T_2^*$. When the resonance field is detuned by $\delta B$, the average macroscopic magnetization undergoes a circular motion in the transverse plane with a beat frequency $\delta f$. The decay time and $\delta f$ were extracted by fitting the FID data (squares) to a Gaussian damped sinusoidal curve (solid lines). Figure 3(b) shows a plot of $\delta f$ versus $\delta B$. The through-origin linear dependence corroborates the relation $\delta f \propto \delta B$. Figure 3(c) displays the temperature dependence of $T_2^*$ for $\delta B = 6$ and 8 G. The obtained $T_2^*$ of $\sim$115 ns agrees with the value calculated from the observed linewidth and remains practically constant from room temperature to 4.2 K.

We have performed driven coherent spin manipulation and obtained the so-called Rabi oscillations. All measurements were performed by applying a nutation pulse around $+x$ axis of length $\tau$ and measuring the resulting $\langle S_y \rangle$ by the FID amplitude after a dead time of $\sim$80 ns. Several examples of the observed Rabi oscillations are given in Fig. 4(a) at different power levels and temperatures. Below 170 K the Rabi amplitude follows the expected $1/T$ dependence. Above 170 K the additional decrease of the amplitude (up to 40% at 290 K) is observed due to the fact that considerable $T_2$ decay occurs during the measurement dead time. Noticeably, the Rabi oscillations are observable even at room temperature.

The experimental data are well described by a single exponential oscillating function

$$\langle S_y \rangle = S_{y(t=0)} e^{-t/\tau_R} \sin(\Omega_R t). \tag{2}$$

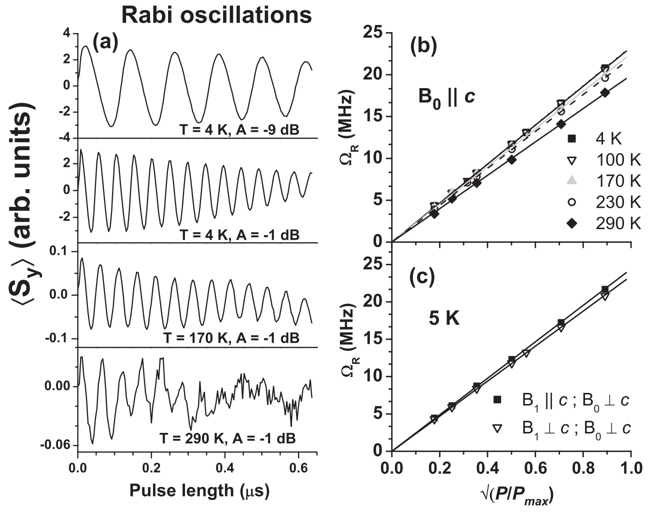

FIG. 4. (a) Rabi oscillations are observed as time evolution of the $\langle S_y \rangle$ component as a function of pulse duration at different power levels and temperatures. (b) Linear dependence of the Rabi frequency ($\Omega_R$) on the microwave amplitude at 4, 100, 170, 230, and 290 K. (c) Orientation dependence of $\Omega_R$ measured at 5 K for two microwave field ($B_1$) directions.

The Rabi frequency $\Omega_R$ and a damping constant $\tau_R$ are determined by fitting the data to Eq. (2). In Fig. 4(b) the Rabi frequency is plotted against the microwave amplitude for temperatures of 4, 100, 170, 230, and 290 K. Since the microwave amplitude is proportional to the square root of the incident power, the $x$ axis is taken as $\sqrt{(P/P_{\mathrm{max}})} = 10^{A/20}$, where $P$ is the power, $P_{\mathrm{max}}$ is the maximum power ($\sim$1 kW), and $A$ is the attenuation in dB. The linear dependence of $\Omega_R$ on the microwave amplitude is consistent with what is expected for Rabi oscillations. Since the $g$ value of Cr:$K_3NbO_8$ is nearly temperature independent [16], the smaller slope of the $\Omega_R$ versus incident power at higher temperatures is due to the smaller $B_1$ field at the sample caused by the smaller resonator $Q$ factor at higher temperatures. The dependence of $\Omega_R$ on the direction of the microwave field $B_1$ at 5 K is displayed in Fig. 4(c). We note that the ratio of $\Omega_R$ between $B_1 \| c$ and $B_1 \perp c$, $(\Omega_{R,\|})/(\Omega_{R,\perp})$, deviates from the expected $g_\| / g_\perp$ ratio and is likely due to the small changes in the resonator $Q$ factor with the sample orientation. However, this small directional dependence of $\Omega_R$ on the microwave field confirms the quasi-isotropic nature of our system. In addition, we have also checked the directional dependence of $\Omega_R$ on the external field $B_0$ and find no difference between the two orientations (not shown here).

The variation of Rabi decay time ($\tau_R$) with drive amplitude at different temperatures is shown in Fig. 5(a). With decreasing microwave power $\tau_R$ increases and then saturates in the low power limit regardless of temperature. In addition, the saturation value of $\tau_R$ increases strongly upon cooling from 290 to 100 K and then remains more or less constant between 100 and 4 K. This behavior resembles the temperature dependence of $T_2$ [see Fig. 2(b)], indicating that $\tau_R$ is restricted by a $T_2$ mechanism. As in Ref. [14] this can be explained by a model based on a stochastic field with a normalized distribution $\beta$ [19,20],

$$1/\tau_R = \beta \Omega_R + 1/2T_2. \tag{3}$$

In our case, this stochastic field can arise from the modulation of the superhyperfine couplings and the radiation

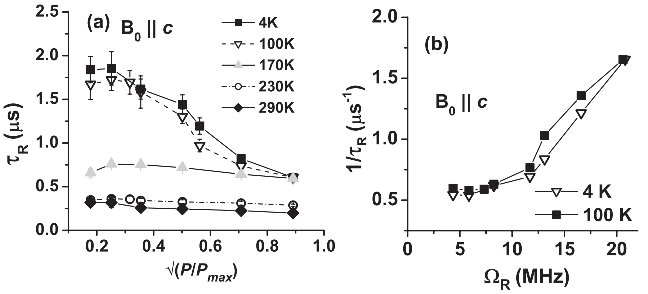

FIG. 5. (a) Rabi oscillations damping time $\tau_R$ as a function of microwave amplitude at five temperatures for $B_0 \| c$ orientation. (b) Rabi oscillations damping rate as a function of $\Omega_R$ at 4 and 100 K for $B_0 \| c$ orientation.

induced changes in the dipolar field [20]. We find that at high temperatures $\tau_R \sim 2T_2$ as expected. In the low temperature range a marked dependence of the Rabi oscillations decay rate on the Rabi frequency or the amplitude of the $B_1$ field is observed. However, this dependence [see Fig. 5(b)] does not show the simple linear dependence from Eq. (3) which was observed in $AlO_4^-$ and $E'$ centers in silicate [20,21], and extrapolates to about 2 $\mu$s at temperatures below 100 K, which is somewhat shorter than the observed $T_2$ (2.7–10 $\mu$s) in this range [see Fig. 2(b)]. We tentatively ascribe this to the larger role played by the $^{39}$K superhyperfine interactions in our system.

The single-qubit figure of merit $Q_M$, defined as $Q_M = \Omega_R T_2/\pi$ [22], estimates the efficiency of a quantum device. Using a $T_2$ time of 10 $\mu$s we obtain ~500 coherent single-qubit operations at liquid helium temperature, implying that $Cr^{5+}$ doped $K_3NbO_8$ is a viable electron-spin qubit. One way to improve the $Q_M$ is to increase the $B_1$ by going to higher microwave power. Even though the $T_2$ of $Cr:K_3NbO_8$ is smaller than that of nitrogen-vacancy centers in diamond [9,10], it is comparable to that of the rare-earth qubits [14] and molecular magnets [13]. As mentioned earlier, the spin decoherence in our system is likely due to the superhyperfine interactions with $^{39}$K nuclei. This hints a possibility of synthesizing samples with even longer coherence time. For example, replacement of $^{39}$K by $^{41}$K reduces the superhyperfine coupling by nearly a factor of 2. We have also succeeded in synthesizing $KCaCrO_8$, which should reduce the superhyperfine interactions due to $^{39}$K by two thirds.

Qubits could be coupled either by dipolar (as in [9]) or by exchange interactions that are of the order of few Kelvin in this system [23]. We have observed that at concentrations higher than 5%, we do form Cr-Cr exchange-coupled triplet pairs, which should in principle enable clustering of several qubits. Such clusters could be further coupled by either dipolar or exchange interactions.

For the present studies, sub-mm sized single crystals were synthesized from solution. In future studies, this technique will be modified to allow precipitation of nanocrystals in areas designed by lithography on an electronic circuit. The qubits could be entangled via photons when integrated in microcavities or via current oscillations if spin detection is done by electronic transport. It is important to note that, in contrast to the 2DEG-based quantum dots where the free electron overlaps over the dot's nuclei, the Cr spins interact only with the neighboring nonzero spin nuclei of the crystal. Spin detection can be done in several ways, for instance by optical detection [24], single-electron transistors [25], nanoSQUIDs [26], or microwave detection by means of SQUID [27] or Hall probes [28]. The quasi-isotropic magnetic character of the Cr spins demonstrated here is relevant for most practical implementations when a controlled positioning of the spins is hard to achieve. Therefore, we consider this novel material to be potentially well suited for integration with standard nanofabrication methods used for on-chip studies.

In conclusion, we have reported on the observation of Rabi oscillations over 4–290 K in $Cr:K_3NbO_8$, an essentially pure $S = 1/2$, metal-oxide system. We find the intrinsic phase-coherence time $T_2 \approx 10$ $\mu$s and the single-qubit figure of merit $Q_M \approx 500$ at liquid helium temperature. Our results demonstrate that the transition metal-oxide-based spin systems hold high potential for quantum information applications.

The authors acknowledge the State of Florida, NSF Cooperative Agreement Grant No. DMR-0084173, and the NSF Grants No. DMR-0520481, No. NIRT-0506946, NSF-CAREER No. DMR-0645408, No. NHMFL-IHRP-5059, the DARPA Grant No. HR0011-07-1-0031, and the Alfred P. Sloan Foundation for financial support. K. Y. C thanks H. Nojiri for helpful discussions.

[1] D. P. DiVincenzo, Science **270**, 255 (1995).
[2] D. Loss and D. P. DiVincenzo, Phys. Rev. A **57**, 120 (1998).
[3] J. R. Petta *et al.*, Science **309**, 2180 (2005).
[4] F. H. L Koppens *et al.*, Nature (London) **442**, 766 (2006).
[5] B. Kane, Nature (London) **393**, 133 (1998).
[6] J. J. L. Morton *et al.*, Nature Phys. **2**, 40 (2006).
[7] T. A. Kennedy *et al.*, Appl. Phys. Lett. **83**, 4190 (2003).
[8] I. Popa *et al.*, Phys. Rev. B **70**, 201203(R) (2004).
[9] R. Hanson *et al.*, Phys. Rev. Lett. **97**, 087601 (2006).
[10] T. Gaebel *et al.*, Nature Phys. **2**, 408 (2006).
[11] L. Childress *et al.*, Science **314**, 281 (2006).
[12] S. Hill *et al.*, Science **302**, 1015 (2003).
[13] A. Ardavan *et al.*, Phys. Rev. Lett. **98**, 057201 (2007).
[14] S. Bertaina *et al.*, Nature Nanotechnology **2**, 39 (2007).
[15] N. S. Dalal *et al.*, J. Chem. Phys. **74**, 1916 (1981).
[16] B. Cage *et al.*, Anal. Chem. **71**, 1951 (1999).
[17] S. Nellutla *et al.* (to be published).
[18] A. Schweiger and G. Jeschke, *Principles of Pulse Electron Paramagnetic Resonance* (Oxford University Press, Oxford, 2001).
[19] R. N. Shakhmuratov, F. M. Gelardi, and M. Cannas, Phys. Rev. Lett. **79**, 2963 (1997).
[20] S. Agnello *et al.*, Phys. Rev. A **59**, 4087 (1999).
[21] R. Boscaino, F. M. Gelardi, and J. P. Korb, Phys. Rev. B **48**, 7077 (1993).
[22] D. P. DiVincenzo, Fortschr. Phys. **48**, 771 (2000).
[23] B. Cage and N. S. Dalal, Chem. Mater. **13**, 880 (2001).
[24] J. Berezovsky *et al.*, Science **314**, 1916 (2006).
[25] H. B. Heersche *et al.*, Phys. Rev. Lett. **96**, 206801 (2006).
[26] J.-P. Cleuziou *et al.*, Nature Nanotechnology **1**, 53 (2006).
[27] B. Cage *et al.*, Appl. Phys. Lett. **87**, 082501 (2005).
[28] G. de Loubens *et al.*, J. Appl. Phys. **101**, 09E104 (2007).